ARTICLE

Dissociative Photoionization of Heterocyclic Molecule-Morpholine under VUV Synchrotron Radiation†

Wen-tao Song, Yong-jun Hu*, Shan Jin, Yu-jian Li

MOE Key Laboratory of Laser Life Science & Institute of Laser Life Science, and Guangzhou Key Laboratory of spectral analysis and functional probes, College of Biophotonics, South China Normal University, Guangzhou 510631, China

(Dated: Received on April 8, 2019; Accepted on April 20, 2019)

The radiation damage of biomolecules, in particular with aliphatic compound, has been extensively studied. Morpholine is a typical six-membered aliphatic heterocyclic compound. In the present work, photoionization and dissociation of the morpholine monomer and subsequent fragmentations have been investigated by synchrotron vacuum ultraviolet photoionization mass spectrometry and theoretical calculations. The vertical ionization energy of morpholine monomer is 8.37±0.05 eV, which agrees reasonably well with a theoretical value 8.41 eV of morpholine. Experimentally observed fragmentation of morpholine (m/z=87 amu) gives rise to m/z=86 amu, m/z=57 amu, and m/z=29 amu. Based on experimental and theoretical results, it is found that the m/z=86 amu is produced by losing H atom, the m/z=57 amu is formed by the elimination of CH_2O with a ring-opening process, the m/z=29 amu is generated by further dissociation of the fragment m/z=57 amu $(C_3H_7N)^+$ by the elimination of C_2H_4. This finding would provide valuable insight into the photo-damage of aliphatic compounds, which may be related to living cells and other biological system.

Key words: Photoionization, Dissociation, Morpholine, Gas phase

I. INTRODUCTION

The interactions of high energy radiation, ions and radical with biomolecules, in particular with the DNA fragment, pyrimidine base and aliphatic molecules, have been extensively studied to uncover effects of photoionization and dissociative photoionization in radiation damage of living cells and other biological system. The sun emits visible light and infrared radiation, which are not considered harmful to humans [1]. Exposure to sun with living under an ultraviolet-rich condition causes unwanted photo-damage [2]. An increasing number of people are exposed to artificial source of ultraviolet radiation used in industries, commercial settings and leisure activities. In recent decades, the problem of the mechanism of the radiation damage is still unsolved [3−9].

Morpholine is a typical six-membered aliphatic heterocycle with the molecular formula $HN(CH_2CH_2)_2O$. Morpholine and its derivatives are used in the synthesis of numerous pesticides, chemicals and drugs. It has been known as a chemical precursor or catalyst in many organic syntheses due to the nucleophilic nitrogen lone pair [10]. Substituted morpholines display anesthetic properties, and the morpholine derivative, amorolfine, is found to be used as an antifungal drug [10]. Furthermore, the morpholine ring structure is an important heterocycle present in many compounds of biological and pharmaceutical relevance [11]. However, to our knowledge, no studies related to the dissociative photoionization channel of morpholine have been reported.

The more stable structures of morpholine are known to exist as a chair form with the N−H bond arranged in an axial (Ax) and equatorial (Eq) conformation in ground state [12−17]. As we know nitrogen and oxygen form polar bond in morpholine and with lone pairs electron, it is a typical model to understand C−N and C−O bond breaking process in the symmetrical heterocyclic molecule. Particularly, the dissociative photoionization for the ring molecules is different from the chain molecule. The presence of a heteroatom in morpholine shifts the electron density of the chemical bond more towards the heteroatom, which leads to a polarized bond, effectively weakening the adjacent bonds.

It is known that the VUV single photon ionization of a neutral species would generate an electron and the excess internal energy remains in the cations (rovibrational states), which leads to further fragmentation. Continuously tunable VUV light is available at synchrotron, which enables the internal energy to be tuned and the fragments at different photon energies are ob-

†Part of the special issue for "the 19th International Symposium on Small Particles and Inorganic Clusters".

*Author to whom correspondence should be addressed. E-mail: yjhu@scnu.edu.cn

served [18]. The internal energy is connected with the ionization process and the VUV light energy and it determines its fragmentation energy and time scale. There is no doubt that a tunable laser of VUV soft ionization should be controlled by a large degree of photon energy to probe the different reaction coordinate regions [19]. It is very powerful to combine tunable synchrotron VUV radiation with the molecular beam and the pulsed field ionization detection techniques to study the photoionization and dissociative photoionization processes of molecules [20−24].

In the present work, we studied photoionization efficiency (PIE) curves of some additional ion resulting from the dissociative photoionization of morpholine in the photon energy region of 8−15 eV. From these PIEs and photoionization mass spectra, we can derive the energetics and mechanisms during the dissociation process. By combining with high level *ab initio* calculation, the various dissociation channels of morpholine are established.

II. METHODS

A. Experimental methods

The experimental apparatus has been described previously [25−27]. Photoionization mass spectrometry (PIMS) measurements have been performed on the Atomic and Molecular Physics Beamline (U14A) with the supersonic expansion molecular beam/a reflection time-of-flight mass spectrometer (RTOFMS) system at the National Synchrotron Radiation Laboratory (NSRL) in Hefei, China. The synchrotron radiation from an undulator-based U14A beamline of 800 MeV electron storage ring is dispersed with 6 m length monochromator, which is equipped with three gratings (370, 740, and 1250 grooves/mm, Horiba Jobin Yvon). Three gratings cover the photon energy from 7.5 eV to 22.5 eV for 370 grooves/mm, 15 eV to 45 eV for 740 grooves/mm, and 36 eV to 124 eV for 1250 grooves/mm, respectively. In this experiment, photon energies are within the limits of 7.5−22.5 eV with a resolution power of 3000 at 15.90 eV and a photon flux with 8×10^{12} photons/sec. The synchrotron light was directed to pass through an argon rare-gas filter to eliminate higher order harmonics produced by the undulator. The sample molecules in the beam were photoionized by the monochromatic synchrotron radiation and the produced ions are detected by a time-of-flight mass spectrometer.

Liquid morpholine (>98% pure) (CAS #110-91-8) was purchased from Aladdin-Reagent company (Shanghai, China) and used without further purification. Both the bubbling procedure and the carrier gas were necessary because of the low vapor pressure of the sample. In the process of experiments, the pressures of the source chamber and the ionization chamber were respectively kept in the range between 2.5×10^{-2} and 2.5×10^{-4} Pa. The species were expanded to form a molecular beam through a 70 μm diameter nozzle and a 2 mm diameter skimmer. The monochromatic VUV radiation is perpendicular to the supersonic molecular beam for ionization. Mass-analysis of the produced ions was performed using a RTOF-MS which is mounted perpendicular to the plane direction determined by the molecular and VUV photon beams; a pair of microchannel plates (MCPs) work in pulse count mode (the repulsion voltage of the TOFMS is a pulsing voltage) were used to collect and detect ions. Signals were transferred to a computer for further processing after pre-amplifying (VT120C, EG&G, ORTEC). The PIE curves of the photon ions were acquired by scanning the monochromator with an energy increment about 50 MeV, and the time of data acquisition for each energy point was 20 s. In order to normalize the ion signals, we used silicon photodiode (SXUV-100, International Radiation Detectors, Inc) to monitor the intensity of photons simultaneously.

B. Computational details

The Gromacs 5.0, MOPAC 2012, GAUSSIAN 09 and ORCA 3.0.3 program packages were used as the theoretical calculations to determine the most stable configuration of morpholine [28−31]. The Gaussian 09 and Gaussian 03 software suites were used for all the following calculations of the dimer and its fragments. The energy of these systems can be determined better by the use of the Møller-Plesset perturbation theory [32]. Therefore, geometry optimizations of the parent cluster, intermediate (INT) ions, and fragments ions were performed by M06-2X theoretical functional based on the 6-311++G(d,p) basis set and with the second order Møller-Plesset perturbation (MP2) theoretical functional by use of the 6-311+G(2d,2p) basis set for reliable energies. The relative energies and the detailed information on the reaction pathways and geometry optimizations of neutral and ionic were also calculated by the MP2 theory at the 6-311++G(d,p) basics set. The appearance energy (AE) of the ionic fragment is conformed to AE=$E_{\max}-E_0$, where the $E_{\max}$ is the highest energy barrier of the corresponding ionic fragment in the formation pathway and the E_0 refers to the absolute energy of neutral [33, 34]. Zero-point energy (ZPE) corrections were also evaluated from the theoretical calculations. The local minimum geometry of the transition state (TS) was optimized at the M06-2X level with the 6-311+G(d,p) basis set to obtain the relative energies more precisely on the reaction paths. All relative energies were zero-point energy (ZPE)-corrected. The calculated interaction energies were corrected for basis set superposition errors (BSSEs) using the scheme of Boys and Bernardi counterpoise correction, as described in the Gaussian program.

The corrected Kohn-Sham-density functional theory (KS-DFT) calculations, which can reliably predict the

DOI:10.1063/1674-0068/cjcp1904068

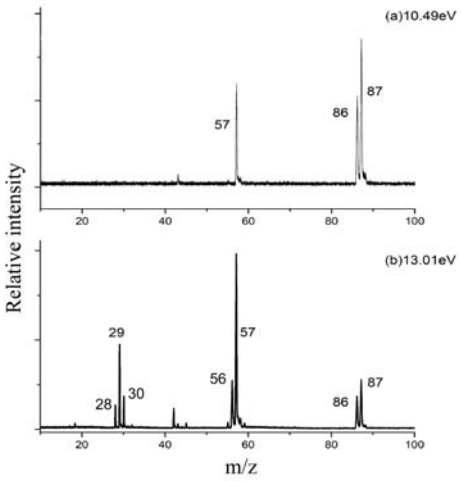

FIG. 1 Photoionization mass spectra of morpholine at VUV photon energies of (a) 10.49 eV and (b) 13.01 eV.

corresponding ionization potentials, were carried out to calculate the energies of the highest occupied orbitals [35−37]. The natural bond orbitals (NBO) calculated at the MP2/6-311++G(d,p) level, at the same calculation level, Laplacian bond order (LBO) were worked out using Multiwfn software. LBO has a direct correlation with the bond polarity, the bond dissociation energy and the bond vibrational frequency. Moreover, LBO is particularly suitable for organic system. The natural bond orbitals (NBO) are calculated at the MP2/6-311++G(d,p) level. In this paper, we report the three highest occupied molecular orbital (HOMO) eigenvalues of the neutral dimers using seven DFT functionals.

III. EXPERIMENTAL RESULTS

A. Photoionization mass spectroscopy

FIG. 1 shows the photoionization mass spectra of morpholine and its fragmentation at 10.49 and 13.01 eV in a supersonic expansion, respectively. To avoid the influence of the fragmentation from the larger clusters, the morpholine ions are detected under the supersonic expansion with a low concentration, of which only the monomer morpholine ions can be seen. Through the VUV one-photon ionization, seven main mass spectral peaks have been seen. The peak at m/z=87 amu is attributed to the parent ion of the morpholine monomer $C_4H_9NO^+$. There are six main mass channels in the mass spectra: $C_4H_8NO^+$ (m/z=86 amu), $C_3H_7N^+$ (m/z=57 amu), $C_3H_6N^+$ (m/z=56 amu), CH_4N^+ (m/z=30 amu), CH_3N^+ (m/z=29 amu), and CH_2N^+ (m/z=28 amu). Compared with the mass spectrum of the morpholine under VUV radiation at 10.49 eV, there are some new peaks appearing at m/z=56 amu, m/z=30 amu, m/z=29 amu and, m/z=28 amu with the incident photon energy of 13.01 eV.

In general, the photoionization process process follows the Franck-Condon principle. Fragment m/z=86 amu $(C_4H_8NO)^+$ could originate from the monomer according to the following reaction,

$$\begin{aligned} C_4H_9NO + h\nu_{VUV} &\rightarrow (C_4H_9NO^+)_{vip} + e^- \\ &\rightarrow C_4H_8NO^+ + H + e^- \quad (1) \end{aligned}$$

where the "vip" represents the vertical ionized point. The excess energy here can be converted into kinetic energy of the ejected electron. The reaction pathway (1) reveals that the hydrogen loss occurs as the Franck-Condon cation evolves to the adiabatic state after the vertical ionization. The ionic fragments with m/z=57 amu are the $C_\alpha-C_\beta$ bond dissociation and ring opening product, *i.e.*, $C_3H_7N^+$, which is generated via the reaction below,

$$\begin{aligned} C_4H_9NO + h\nu_{VUV} &\rightarrow (C_4H_9NO^+)_{vip} + e^- \\ &\rightarrow C_3H_7N^+ + CH_2O^* + e^- \quad (2) \end{aligned}$$

where the $(C_4H_9NO^+)_{vip}$ are the Franck-Condon cations with excess energy [39]. The new fragment m/z=29 amu (CH_3N^+) is generated by further dissociation of the fragment m/z=57 amu ($C_3H_7N^+$). The C−N bond of $C_3H_7N^+$ is broken and the reaction can be represented as

$$C_3H_7N^+ \rightarrow CH_3N^+ + C_2H_4^* \quad (3)$$

B. Photoionization efficiency curve

The photoionization efficiency (PIE) curves for the monomer and main fragmentations were recorded by integrating the area of each mass spectral peak at different photon energies. FIG. 2 shows the PIE spectra of the morpholine monomer ion $C_4H_9NO^+$ (m/z=87 amu) and the main fragment ions $C_4H_8NO^+$ (m/z=86 amu), $C_3H_7N^+$ (m/z=57 amu), CH_3N^+ (m/z=29 amu) and CH_4N^+ (m/z=30 amu). The PIE spectra of $C_3H_6N^+$ (m/z=56 amu) and CH_2N^+ (m/z=28 amu) are displayed in the FIG. S2 (supplementary materials). In the present study, most AEs in PIE curves have been extrapolated by intersection of a linear section with the x-axis and some (*e.g.* 8.37, 9.50, and 9.80 eV) were reasonably taken as the first values out of the baseline [38, 39]. Furthermore, the experimental uncertainties in the low-energy region are 0.05 eV, and 0.1 eV in a higher photon energy range (4−13 eV), respectively. Note that there are differences between the calculated and experimental results, which could be caused by the effects of thermal energy, kinetic shifts, fragment excitation, *etc.*, as thoroughly described by Baer and co-workers over the past few decades [40−43].

FIG. 2 shows the PIE curves of the parent ion $C_4H_9NO^+$ (m/z=87 amu) and the fragment ions $C_4H_8NO^+$ (m/z=86 amu), $C_3H_7N^+$ (m/z=57 amu), CH_3N^+ (m/z=29 amu) and CH_4N^+ (m/z=30 amu), respectively. In the PIE curve of $C_4H_9NO^+$, the onset

DOI:10.1063/1674-0068/cjcp1904068

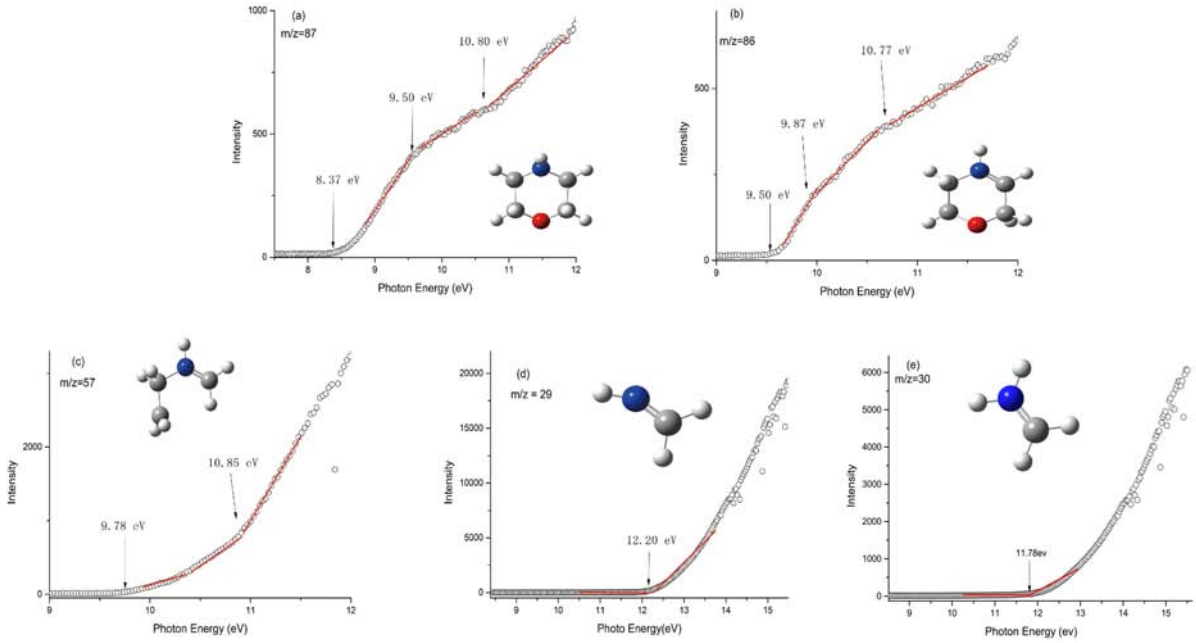

FIG. 2 PIE spectra of the morpholine monomer and fragments at mass channels (a) m/z=87 amu, (b) m/z=86 amu, (c) m/z=57 amu, (d) m/z=29 amu, (e) m/z=30 amu. Each mass channel corresponds to different fragments.

of ionization of $C_4H_9NO^+$ is 8.37±0.05 eV. The appearance energy (AE) of the fragment ions of the morpholine monomer are determined by the onset in each PIE curve, for example the AEs of $C_4H_8NO^+$, $C_3H_7N^+$, CH_3N^+ and CH_4N^+ are determined as 9.50±0.05 eV, 9.78±0.05 eV, 12.20±0.05 eV and 11.78±0.05 eV, respectively. All the AE values are listed in Table I. Note that the PIE curve for m/z=87 amu becomes less intense at 9.50±0.05 eV, which is the same value as the adiabatic ionization energy (AIE) of its daughter ions at m/z=86 amu. The coincidence suggests that one new fragmentation path opens and consumes the parent ions at the same time. In each PIE curves of FIG. 2, one or two inflection points can also be observed, for instance, 9.87 and 10.77 eV in FIG. 2(b) and 9.78 and 10.85 eV in FIG. 2(c). The integral intensity of a mass channel becomes less intense or flat (negative contribution), and meanwhile at the same inflection point (same photon energy), the signal intensity increases sharply for another fragment cation. These would indicate the closure of some reaction pathways, which could generate the fragment at this mass channel or another new competitive fragmentation path opening for its parent ions. However, low photoionization cross-sections can also be responsible for the flattening of the curve. Similarly, the opening of new reaction pathways related to a fragment will make a positive contribution to its mass channel, where the signal becomes stronger. Therefore, a detailed analysis of reaction paths is required to explain those inflections points in each PIE curve.

In this work, all the AE of each PIE curve can be determined by using a linear least-squares fit in the threshold region. The thermal effect is ignored in our data processing because of the supersonic nozzle expansion condition. This kind of method for data analysis has been successfully carried out in the study on dissociative photoionization processes previously [23, 24, 38, 39].

TABLE I Experiment AEs compared with the calculation value at MP2/6-311++G (2d,2p) levels.

Species	(m/z)/(amu)	IEs/eV	
		MP2	Expt.
$C_4H_9NO^+$	87	8.41	8.37±0.05
$C_4H_8NO^+$	86	9.51	9.50±0.05
$C_3H_7N^+$	57	9.60	9.78±0.05
CH_3N^+	29	12.25	12.20±0.05
CH_4N^+	30	11.80	11.78±0.05

IV. DISCUSSION

A. Structures of the neutral and ionic morpholine

Previous reports have revealed that there are four possible conformational landscapes of the morpholine. Both the skew-boat and the chair conformations are found to be stable, and four conformations distinguish from the N−H bond lying either axial or equatorial relative to the boat and chair ring (Eq-chair, Ax-chair, Ax-boat and Eq-boat) [12, 43]. The structures of mor-

DOI:10.1063/1674-0068/cjcp1904068

pholine were optimized at the ωB97X-D/cc-pVTZ levels of theory. The relative energies were calculated at MP2/aug-cc-pVTZ level. The theoretical calculation confirmed that Eq-chair is the lowest energy conformer, and it is regarded as the benchmark in FIG. S1 (supplementary materials). The most stable conformer is the chair structure (estimated ca. 97%) in the molecular beam with consideration of low experimental temperature [45] (∼10 K) caused by the supersonic nozzle expansion.

The chair conformer is much more symmetric and stable (by ca. 0.26 eV) than the skew-boat conformer, which indicates the chair conformer could be favorable in the gas phase. However, the energy difference between two chair conformers (axial and equatorial) is only 0.05 eV and the axial conformer is more stable since the existence of N−H equatorial bond can weaken the interaction of hydrogen atoms in Eq-chair conformer, this implies that these two chair conformers are concomitant in gas phase.

FIG. 3 shows the fully optimized geometries of the most stable morpholine monomer in neutral, ionic states and its intermediate (INT), transition state (TS) and stable fragments at the ωB97X-D/cc-pVTZ levels of theory. These computational methods have been successfully applied to carry out potential energy surface calculations [49−52]. In order to achieve the higher accuracy, the whole of relative energies (the stable structures, TS and INT found in the path search) were recalculated at the MP2/6-311++G(2d,2p) levels and further used to analyze the experimental results. The IE of the most stable conformer of morpholine is calculated to be 8.41 eV and agrees reasonably well with our measured appearance energy of 8.37 eV shown in the PIE curve for the parent cation in FIG. 2(a). The discrepancy of 0.04 eV between theoretical and experimental results is likely to be the unfavorable Franck-Condon factors. This implies that, on removal of an electron from the nitrogen lone pair, the morpholine cations would be the single-electron structure.

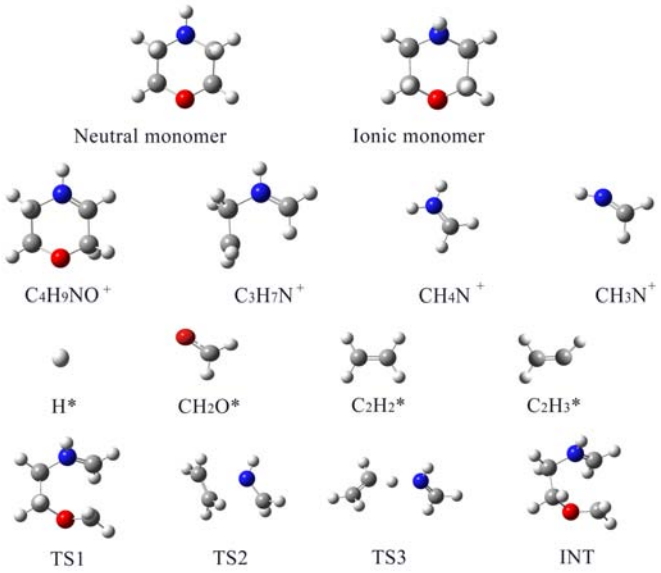

FIG. 3 The geometries of the neutral and ionic monomer, INT, TS and fragment at ωB97X-D/cc-pVTZ.

B. Highest occupied molecular orbitals (HOMO)

According to the results of the molecular orbital (MO) analysis of the neutral morpholine at MP2/6-311++G(2d,2p) (Pop=NBO) level, the three highest occupied molecular orbitals (HOMO) can be assigned [46−48]. The HOMO is located on nitrogen atom of the ring; HOMO−1 is located on ether oxygen of the ring; HOMO−2 is populated on the carbon atom next to the nitrogen atom of the ring. As shown in FIG. 4, the electron densities of HOMO are contributed from the mixture of the non-bonding p orbital of N atom and the p orbital of the neighboring C atom while the N atom's non-bonding p orbital is dominant. The HOMO of morpholine in its ground state is predominantly the nonbonding nitrogen lone pair orbital n, which implies that the electron will be mainly removed from the N atom when the morpholine molecule is vertically ionized. There is a multiple hyperconjugation between the N_{LP^*}, C−N orbital and C−C orbital. When the electron is ejected from the N atom, the electron of C−C orbital can transfer toward N atom resulting from the multiple hyperconjugation. Thus, removing the electron from these orbital results in weakening the C−C bond in the ring. Neutral morpholine and their adiabatic state ions are fully optimized at ωB97X-D/cc-pVTZ levels of theory. For the ionic conformer, the C−C distance is 1.60 Å, longer than that of neutral (1.52 Å). It indicates that the C−C bond is weaker after being ionized. The Laplacian bond order (LBO) with Multiwfn software was calculated at the same level to estimate the bond strengths. Table S1 (supplementary materials) shows that LBO of C_1-C_2/C_3-C_4 diminished from 1.177 Å to 0.919 Å when Franck-Condon ions relax to the adiabatic state ions. These theoretical calculation results indicated that the C−C bond would be broken at first. Therefore, the morpholine monomer can be vertically ionized when the VUV photon energy is high enough to eject the electron of the HOMO or HOMO−1 of the morpholine monomer, respectively. When the energy exceeds the barrier of transition state, the C−N bond of the fragment m/z=57 amu breaks, and the fragment further dissociates into m/z=29 amu. Above all, the energy diagram is shown in FIG. 4.

C. Mechanisms of photoionization and dissociation of the neutral morpholine monomer

For the fragmentation of the dissociation of morpholine, the possible formation pathways are depicted in FIG. 4 and FIG. S3 (supplementary materials). Gener-

DOI:10.1063/1674-0068/cjcp1904068

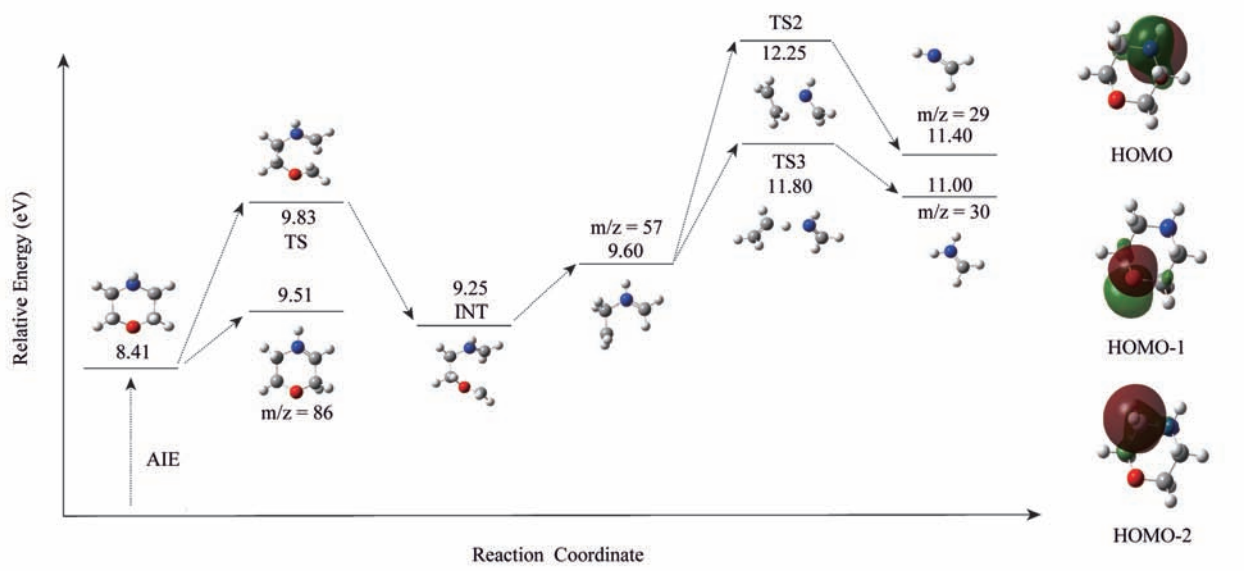

FIG. 4 Energy diagram for the VUV one-photon photoionization and dissociation of the morpholine monomer. The highest occupied molecular orbitals of the neutral are also shown at the MP2/6-311++G(2d,2p) level (the iso density surface is drawn at a value of 0.02).

ally, there are two types of mechanisms for dissociative photoionization: the bond was broken directly or via transition states and intermediate states.

These dissociation channels for morpholine are studied in the photon energy of 13.01 eV, the m/z=57 amu is generated by losing CH_2O neutral, while the m/z=29 amu is generated from m/z=57 amu by the elimination of C_2H_4. The generation of the fragment at m/z=30 amu is a parallel reaction channel with that of the fragment at m/z=29 amu from the one at m/z=57 amu, a proton transfer from the C_α−H group to the nitrogen-atoms while the C_α−N bond cleavage. For the m/z=86 amu, there are three possibilities: breaking of the two different C−H bonds or the cleavage of N−H bond. This is a direct dissociation channel. In the case of possible dissociation channel $C_4H_9NO \rightarrow C_4H_8NO^+ + H^*$, the AIE of $C_4H_8NO^+$ was obtained by,

$$\mathrm{AIE}(C_4H_8NO^+) = E(C_4H_8NO^+) + E(H^*) - E(C_4H_9NO) \quad (4)$$

Theoretical results reveal that the value of AIE was 9.51 eV, which is in good agreement with the experimental value 9.50 eV (FIG. 2). Theoretical calculations confirmed that the H is fissured from C_4−H_9, which needed to surmount an energy barrier. To estimate the bond strength, we calculated the Laplacian bond order (LBO) with Multiwfn software at MP2/6-311++G(2d,2p) level. Table S1 shows that LBOs of C_4−H_9/C_1−H_{11} are smaller than those of other C−H bonds. The electron is removed from the N atom when the molecule is ionized. The ionized N atom would seize the electron from the contiguous carbon atom, this will weaken the C−H and C−C bond strengths. While the former results in the H-losing process, the latter will induce a new channel to be opened. The bond energies of the individual hydrogen atom loss channel are calculated and shown in FIG. S4 (supplementary materials). The result also shows that the H is fission from C_4−H_9.

In the latter fragmentation process, the cleavage of C−C bond occurred firstly in accordance with our expectations in FIG. 4 based on the analysis of the MO shape. Since the C−C bond was significantly weakened in the cation (as evidenced by LBO), it was likely to open the cyclic structure. All structures of fragment, TS1, TS2, TS3, INT and their relative energy are theoretical predicted. FIG. 4 shows that the energy diagram of the reaction path of morpholine under the VUV one-photon ionization. Structure AE can turn into INT through the transition state TS1. Structure TS1 could come from AE by means of the C_3−C_4 bond cleavage. In this process, the cleavage of bond is required and higher energy barriers are predicted to exist. Corresponding TS1 and INT with an energy barrier of 1.42 eV in morpholine cation can be calculated as follows,

$$\Delta E = E(\mathrm{TS1}) - E(C_4H_9NO^+) = 1.42\ \mathrm{eV} \quad (5)$$

After the C_3−C_4 bond cleavage, the C_2−O bond is elongated to 1.411 Å, but the C_1−C_2 bond is shortened to 1.523 Å in TS1. Thereafter, the fragment $C_3H_7N^+$ (m/z=57 amu) could be generated by the dissociation of INT. The C_2−O bond via an INT to $C_3H_7N^+$ (m/z=57 amu), and the AE for $C_3H_7N^+$ (m/z=57 amu) can be calculated as follows,

$$\mathrm{AE}(C_3H_7N^+) = E(\mathrm{TS1}) - E_0 = 9.83\ \mathrm{eV} \quad (6)$$

The result is in excellent agreement with the experimental value, which is measured as 9.78±0.05 eV in the

DOI:10.1063/1674-0068/cjcp1904068

PIE cure of $C_3H_7N^+$ (see FIG. 2).

While at higher photon energy, the fragment $C_3H_7N^+$ (m/z=57 amu) will further dissociate and the fragment CH_3N^+ (m/z=29 amu) is generated. There is a transition state (TS2) related to the cleavage of C−N bond in this process, which possess high energy barrier. In this process, the cleavage of the bond is required to surmount a higher energy barrier of 2.65 eV between TS2 and the fragment $C_3H_7N^+$ (m/z=57 amu).

Thereafter, the fragment CH_3N^+ (m/z=29 amu) could be generated while TS2 was surmounted. The AE for CH_3N^+ (m/z=29 amu) can be calculated as follows,

$$\mathrm{AE}(CH_3N^+) = E(\mathrm{TS2}) - E_0 = 12.25\ \mathrm{eV} \qquad (7)$$

which agrees well with the experimental value measured as 12.20±0.03 eV in the PIE cure of CH_3N^+ (see FIG. 2)

The generation of fragment CH_4N^+ (m/z=30 amu) is regarded as another channel from the $C_3H_7N^+$ (m/z=57 amu), where the H atom of the C−H bond transfers to the N−H group while the C−N bond is broken. A transition state (TS3) displays in this process, and we also perform the intrinsic reaction coordinate (IRC) calculations to confirm that TS3 connects two appropriate local minima in the reaction pathways. The IRC calculations are shown in FIG. S5 (supplementary materials).

Therefore, when the energy exceeds the barrier of TS3, the fragment CH_4N^+ (m/z=30 amu) could be generated. The AE of the fragment CH_4N^+ can be calculated as follows:

$$\mathrm{AE}(CH_4N^+) = E(\mathrm{TS3}) - E_0 = 11.80\ \mathrm{eV} \qquad (8)$$

The result is in agreement with the experimental value, which is measured as 11.78±0.03 eV in the PIE cure of CH_4N^+ (see FIG. 2).

Note that the measured AEs involving a barrier show slightly lower than the theoretical results, it could be attributed to the kinetic shift. The kinetic shift results in the overestimation of threshold energies due to the contribution of excess energy in the transition state necessary to yield rate constants larger than 10^6 s^{-1}. The excess energy in the transition state affects the AEs measurements such that it always causes the threshold energies to be overestimated.

V. CONCLUSION

We have presented the photo-induced photoionization and dissociative photoionization of morpholine by ultraviolet synchrotron radiation PIMS combined with theoretical calculations. The experiments show the AIE of the chair form morpholine is 8.37±0.05 eV in the gas phase. This value agrees reasonably well with a theoretical estimation of 8.41 eV. Four main mass dissociation channels $C_4H_8NO^+$, $C_3H_7N^+$, CH_3N^+ and CH_4N^+ were measured at 9.50±0.05 eV, 9.78±0.05 eV, 12.20±0.05 eV, 11.78±0.03 eV respectively.

The morpholine monomer could be photo-dissociated by breaking C−C, C−O, C−N bonds because of site-selective photoionization, resulting in two distinct fragment ions, *i.e.* CH_3N^+ and $C_3H_7N^+$. When an electron was removed from the HOMO with low photon energy, the C−H bond was broken to generate the $C_4H_8ON^+$ (m/z=86 amu) fragment cation. At higher photon energy, an electron can be ejected from the HOMO−1. The C_α−C_β bond and C−O bond would be broken to generate the $C_3H_7N^+$ (m/z=57 amu) fragment cation. As the photon energy increases, the fragment $C_3H_7N^+$ (m/z=57 amu) will further dissociate to CH_3N^+ (m/z=29 amu) and CH_4N^+ (m/z=30 amu) with the cleavage of C−N bond, which is confirmed experimentally and theoretically. The study conclusions of morpholine can be applied to the aliphatic heterocyclic compound and may be translated to living cells and other biological systems in the future.

Supplementary materials: The four lowest-energy structures of morpholine, distances of atoms in the neutral and cationic morpholine monomer, PIE spectra of the morpholine monomer and fragmentation at mass channels m/z=56 amu and m/z=28 amu, energy diagram for the VUV one-photon photoionization and dissociation of the morpholine monomer, the comparison of the bond energies of the individual hydrogen loss channel and IRC calculation of fragment CH_4N^+ are available.

VI. ACKNOWLEDGMENTS

We thank the Atomic and Molecular Physics Beamline (U14A) at the National Synchrotron Radiation Laboratory for their contribution in the PIMS apparatus and data acquisition system. This work was supported by the National Natural Science Foundation of China (No.U1732146 and No.21273083) and the Scientific and Technological Planning Project of Guangzhou City (No.201805010002).

[1] M. Wlaschek, I. Tantcheva-Poór, L. Naderi, W. Ma, L. A. Schneider, Z. Razi-Wolf, J. Schüller, and K. Scharffetter-Kochanek, J. Photoch. Photobio. B **63**, 41 (2001).
[2] L. Dicelio and I. Joekes, Photoch. Photobio. Sci. **5**, 165 (2006).
[3] M. F. Barbe, M. Tytell, D. J. Gower, and W. J. Welch, Science **241**, 1817 (1988).
[4] R. E. Marc, B. Jones, C. Watt, F. Vazquez-Chona, D. Vaughan, and D. Organisciak, Mol. Vis. **14**, 782 (2008).
[5] D. T. Organisciak and D. K. Vaughan, Prog. Retin. Eye Res. **29**, 113 (2010).
[6] S. Takahashi and M. R. Badger, Trends Plant Sci. **16**, 53 (2011).
[7] D. Fuller, R. Machemer, and R. W. Knighton, Vis. Res. **20**, 1055 (1980).

DOI:10.1063/1674-0068/cjcp1904068

[8] D. T. Organisciak, R. M. Darrow, L. Barsalou, R. A. Darrow, R. K. Kutty, G. Kutty, and B. Wiggert, Invest. Ophth. Vis. Sci. **39**, 1107 (1998).
[9] J. S. Penn, M. I. Naash, and R. E. Anderson, Exp. Eye Res. **44**, 779 (1987).
[10] T. A. A. Oliver, G. A. King, and M. N. R. Ashfold, Chem. Sci. **1**, 89 (2010).
[11] G. Assaf, G. Cansell, D. Critcher, S. Field, S. Hayes, S. Mathew, and A. Pettman, Tetrahedron Lett. **51**, 5048 (2010).
[12] H. Zhan, Y. Hu, P. Wang, and J. Chen, Rsc Adv. **7**, 6179 (2017).
[13] J. J. Sloan and R. Kewley, Can. J. Chem. **47**, 3453 (1969).
[14] J. U. Grabow, H. Ehrlichmann, and H. Dreizler, J. Phys. Sci. **44**, 833 (1989).
[15] N. L. Allinger and J. C. Tai, J. Am. Chem. Soc. **87**, 2081 (1965).
[16] R. W. Baldock and A. R. Katritzky, Tetrahedron Lett. **9**, 1159 (1968).
[17] M. Xie, G. Zhu, Y. Hu, and H. Gu, J. Phys. Chem. C **115**, 20596 (2011).
[18] K. Vékey, *Role of Internal Energy in Mass Spectrometric Fragmentation*, Netherlands: Springer, (1997).
[19] Y. J. Shi, S. Consta, A. K. Das, B. Mallik, D. Lacey, and R. H. Lipson, J. Chem. Phys. **116**, 6990 (2002).
[20] M. Dampc and M. Zubek, Int. J. Mass Spectrom. **277**, 52 (2008).
[21] D. Ghosh, A. Golan, L. K. Takahashi, A. I. Krylov, and M. Ahmed, J. Phys. Chem. Lett. **3**, 97 (2012).
[22] G. Vall-Llosera, M. Coreno, P. Erman, M. A. Huels, K. Jakubowska, A. Kivimäki, E. Rachlew, and M. Stankiewicz, Int. J. Mass Spectrom. **275**, 55 (2008).
[23] J. Guan, Y. Hu, H. Zou, L. Cao, F. Liu, X. Shan, and L. Sheng, J. Chem. Phys. **137**, 124308 (2012).
[24] Y. Tao, Y. Hu, W. Xiao, J. Guan, F. Liu, X. Shan, and L. Sheng, Phys. Chem. Chem. Phys. **18**, 13554 (2016).
[25] I. Polikarpov, L. A. Perles, R. T. de Oliveira, G. Oliva, E. E. Castellano, R. C. Garratt, and A. Craievich, J. Synchrotron Radiat. **5**, 72 (2010).
[26] C. C. Kao, K. Hamalainen, M. Krisch, D. P. Siddons, T. Oversluizen, and J. B. Hastings, Rev. Sci. Instrum. **66**, 1699 (1995).
[27] Z. Wu, W. Zhao, H. Zhang, B. Liu, Y. Xie, and J. Hao, Nucl Tech. **9**, 684 (2009).
[28] M. J. Frisch, G. W. Trucks, H. B. Schlegel, G. E. Scuseria, M. A. Robb, J. R. Cheeseman, G. Scalmani, V. Barone, B. Mennucci, G. A. Petersson, H. Nakatsuji, M. Caricato, X. Li, H. P. Hratchian, A. F. Izmaylov, J. Bloino, G. Zheng, J. L. Sonnenberg, M. Hada, M. Ehara, K. Toyota, R. Fukuda, J. Hasegawa, M. Ishida, T. Nakajima, Y. Honda, O. Kitao, H. Nakai, T. Vreven, J. A. Montgomery Jr., J. E. Peralta, F. Ogliaro, M. Bearpark, J. J. Heyd, E. Brothers, K. N. Kudin, V. N. Staroverov, R. Kobayashi, J. Normand, K. Raghavachari, A. Rendell, J. C. Burant, S. S. Iyengar, J. Tomasi, M. Cossi, N. Regna, J. M. Millam, M. Klene, J. E. Knox, J. B. Cross, V. Bakken, C. Adamo, J. Jaramillo, R. Gomperts, R. E. Stratmann, O. Yazyev, A. J. Austin, R. Cammi, C. Pomelli, J. W. Ochterski, R. L. Martin, K. Morokuma, V. G. Zakrzewski, G. A. Voth, P. Salvador, J. J. Dannenberg, S. Dapprich, A. D. Daniels, O. Farkas, J. B. Foresman, J. V. Ortiz, J. Cioslowski, and D. J. Fox, *Gaussian 09*, Wallingford CT: Gaussian, Inc., (2009).
[29] B. Hess, C. Kutzner, D. Van Der Spoel, and E. Lindahl, J. Chem. Theory Comput. **4**, 435 (2008).
[30] J. J. Stewart, *Stewart Computational Chemistry*, Colorado Springs, CO, USA (2012).
[31] F. Neese, WIRES Comput. Mol. Sci. **2**, 73 (2012).
[32] J. S. Binkley and J. A. Pople, Int. J. Quantum Chem. **9**, 229 (1975).
[33] X. Liu, W. Zhang, Z. Wang, M. Huang, X. Yang, L. Tao, Y. Sun, Y. Xu, X. Shan and F. Liu, J. Mass Spectrom. **44**, 404 (2010).
[34] Y. Pan, L. Zhang, T. Zhang, H. Guo, X. Hong, L. Sheng, and F. Qi, Phys. Chem. Chem. Phys. **11**, 1189 (2009).
[35] P. Politzer and F. Abu-Awwad, Theor. Chem. Acc. **99**, 83 (1998).
[36] P. Politzer, J. S. Murray, and F. A. Bulat, J. Mol. Model. **16**, 1731 (2010).
[37] R. Stowasser and R. Hoffmann, J. Am. Chem. Soc. **121**, 3414 (1999).
[38] W. Li, Y. Hu, J. Guan, F. Liu, X. Shan, and L. Sheng, J. Chem. Phys. **139**, 024307 (2013).
[39] W. Xiao, Y. Hu, W. Li, J. Guan, F. Liu, X. Shan, and L. Sheng, J. Chem. Phys. **142**, 024306 (2015).
[40] Q. Li, Q. Ran, C. Chen, S. Yu, X. Ma, L. Sheng, Y. Zhang, and W. K. Li, Int. J. Mass Spectrom. Ion Proc. **153**, 29 (1996).
[41] T. Baer, B. Sztáray, J. P. Kercher, A. F. Lago, A. Bödi, C. Skull, and D. Palathinkal, Phys. Chem. Chem. Phys. **7**, 1507 (2005).
[42] B. Hornung, A. Bödi, C. I. Pongor, Z. Gengeliczki, T. Baer, and B. Sztáray, J. Phys. Chem. A **113**, 8091 (2009).
[43] B. Sztáray, A. Bödi, and T. Baer, J. Mass Spectrom. **45**, 1233 (2010).
[44] M. Xie, Y. Matsuda, and A. Fujii, J. Phys. Chem. A **119**, 5668 (2015).
[45] P. Carçabal, R. Jockusch, I. Hünig, L. Snoek, R. T. Kroemer, B. Davis, D. Gamblin, I. Compagnon, J. Oomens, and J. Simons, J. Am. Chem. Soc. **127**, 11414 (2005).
[46] T. Shi, D. Yang, Q. Zhu, J. Ge, P. Bai, L. Sheng, G. Wu, and Y. Zhang, Phys. Chem. Chem. Phys. **6**, 2281 (2004).
[47] T. Shi, J. Ge, J. Guo, and Q. Zhu, Chem. Phys. Lett. **397**, 160 (2004).
[48] T. Shi, J. Ge, Y. Zhang, and Q. Zhu, J. Chem. Phys. **120**, 8453 (2004).
[49] L. N. Domelsmith and K. N. Houk, Tetrahedron Lett. **23**, 1981 (1977).
[50] V. Galasso and F. Pichierri, J. Phys. Chem. A **113**, 2534 (2009).
[51] R. Parthasarathi, Y. He, J. P. Reilly, and K. Raghavachari, J. Am. Chem. Soc. **132**, 1606 (2010).
[52] Y. Zhao, J. Yuan, X. Ding, S. He, and W. Zheng, Phys. Chem. Chem. Phys. **13**, 10084 (2011)

DOI:10.1063/1674-0068/cjcp1904068